Long-lived chondroprogenitors are generated by fetal-limb Gli1$^+$ cells and are replenished upon mosaic cell-cycle arrest in the cartilage.

Xinli Qu[1¶], Ehsan Razmara[1¶], Chee Ho H'ng[1], Kailash K. Vinu[1], Luciano G. Martelotto[2,3], Magnus Zethoven[4], Fernando J. Rossello[5,6,7], Ricky W. Johnstone[4], Shanika L. Amarasinghe[1,8,9], David R. Powell[8,10], Alberto Rosello-Diez[1,11-13*]

[1]Australian Regenerative Medicine Institute, Monash University, Clayton, Victoria, Australia.
[2]University of Melbourne Centre For Cancer Research, The University of Melbourne, Melbourne, Victoria, Australia.
[3]Present address: Adelaide Centre for Epigenetics. South Australian immunoGENomics Cancer Institute. University of Adelaide, Adelaide, South Australia, Australia.
[4]Translational Haematology Program, Peter MacCallum Cancer Centre, Melbourne, Victoria, Australia.
[5]Murdoch Children's Research Institute, The Royal Children's Hospital, Melbourne, VIC 3052, Australia
[6]Novo Nordisk Foundation Center for Stem Cell Medicine, Murdoch Children's Research Institute, Melbourne, VIC 3052, Australia.
[7]Department of Clinical Pathology, University of Melbourne, Melbourne, VIC, Australia.
[8]Monash Genomics and Bioinformatics Platform, Monash University, Clayton, Victoria, Australia.
[9]Present address: Biomedicine Discovery Institute, Monash University, Clayton, Victoria, Australia.
[10]Monash eResearch Centre, Monash University, Clayton, Victoria, Australia.
[11]Department of Physiology, Development and Neuroscience, University of Cambridge, Cambridge, UK.
[12]Department of Genetics, University of Cambridge, Cambridge, UK.
[13]Centre for Trophoblast Research, University of Cambridge, Cambridge, UK.

[¶]Equal contribution

***Correspondence:**
ar2204@cam.ac.uk, alberto.rosellodiez@monash.edu

Keywords: Gli1, Pdgfra, growth plate, endochondral ossification, chondroprogenitors, long bones, limb growth, skeletal stem cells, perichondrium, catch-up growth.

Abstract

Key questions in organ development and regeneration revolve around the origin and regulation factors of the progenitor cells that fuel organ growth[1]. The cartilage progenitors that drive long-bone growth display a postnatal switch in their behaviour, from short-lived progenitors to self-renewing, long-lived ones[2]. However, it is unclear whether these are distinct populations with different origins, or the same population changes over time due to intrinsic/extrinsic factors, or there is no real behavioural switch, just differential proximity to a supportive niche. The multiple candidates of cartilage stem-cell/progenitors that have been recently described add more complexity to this field, as it is unclear how much spatio-temporal overlap there is between these populations. Here, using lineage tracing, single-cell transcriptomics and label-retention assays during normal and compensatory growth, we show that Gli1$^+$ cells in fetal cartilage are long-lived chondroprogenitors that remain dormant until postnatal stages. Moreover, Pdgfra$^+$ cells outside the cartilage contribute only to short-term chondroprogenitors in normal conditions, but become Gli1-expressing and increase their cartilage contribution in response to cartilage cell-cycle arrest. These findings shed light on the long-standing question of the origin and regulation of long-lived cartilage progenitors, laying the groundwork for potential future approaches to generate cartilage reparative cells in vivo.

Introduction

Long bones grow via a transient cartilage template that is progressively replaced by bone[3]. Cartilage cells (chondrocytes) undergo progressive end-to-centre differentiation, starting as resting/reserve chondrocytes that are progressively recruited into the proliferative pool (flat cells arrayed in columns), which eventually enlarge and differentiate to hypertrophic chondrocytes (HTCs). Some HTCs die, while others transdifferentiate into osteoblasts (bone-laying cells) that replace the cartilage with bone, forming the primary ossification center[4,5]. Osteoblasts can also migrate, along with blood vessels, from the perichondrium[6], a connective tissue layer that surrounds the cartilage and has been shown to be a stem-cell niche[7]. A secondary ossification centre (SOC) forms later (~postnatal day 7 in the mouse) at both ends of the skeletal element, so that the growth cartilage gets 'sandwiched' into a so-called growth plate by both ossification centres.

Maintaining the size and structure of the growth plate requires refined mechanisms of control. The size of the proliferative zone is maintained ~constant due to a very well described negative feedback loop between Indian hedgehog (IHH) and Parathyroid hormone related peptide (PTHrP), which balances proliferation and differentiation[4]. But other mechanisms of control are not so well known, especially regarding the resting-to-proliferative transition. Maintenance of the cartilage (and hence bone growth) requires that the continuous cartilage destruction happening at the bone centre be counterbalanced by new chondrocytes arising from chondroprogenitors (CPs) in the reserve/resting zone. In fetuses and neonates, CPs located in the reserve zone do not self renew[2], so that when one is recruited into a proliferative column, its lineage gets soon exhausted, leading to short clonal columns (Suppl. Fig. 1). However, sometime after the SOC is formed, CPs start to self-renew, giving rise to long clonal columns[2]. While some of these mid- and long-lived CPs (LLCPs) are marked postnatally by PTHrP[8] and FoxA2[9], the fetal precursors of LLCPs may express other markers. Initial studies used *Col2a1* as a general marker of chondrocytes and CPs to show that a subset of the cells expressing *Col2a1-CreER* at embryonic day (E) 11.5 give rise to chondrocytes columns at least up to postnatal day (P) 21, but there were two caveats[10]. First, at those very early stages, before the cartilage template is fully formed, *Col2a1* also marks cells in the perichondrium, casting doubts on the cartilage vs. perichondrium origin of the long-lived progenitors. Second, analysis of cartilage contribution beyond P21 was only done after postnatal activation of *Col2a1-CreER,* raising the possibility that true LLCPs only arise postnatally. Later, it was proposed that Hoxa11$^+$ cells in the stromal tissues surrounding the fetal cartilage templates are skeletal stem cells that give rise to cartilage, bone and fat progenitors throughout life[11]. However, the available data suggest that less than 50% of the 8-week-old growth-plate chondrocytes derive from E13.5-labelled Hoxa11-lineage[11], raising the question of what other fetal population(s) give rise to the LLCPs. Moreover, since *Hoxa11* is mostly expressed towards the interzone at the distal zeugopod (i.e., wrist and ankle)[11], it remains to be determined whether a more general marker can identify this population in other long bones. A potential candidate is Platelet-derived growth factor receptor alpha (Pdgfra), as most Hoxa11$^+$ cells co-express *Pdgfra* at all stages analysed[11]. Regarding the potential contribution of external cells, it has been shown that Hes1$^+$ cells surround the early cartilage anlagen and their lineage contributes to perichondrium and cartilage (at least up to P21)[12] when labelled at E10.5, but not when labelled at E12.5 or E14.5, revealing that Hes1 is not a permanent general marker of fetal stromal cells contributing to LLCPs either. Lastly, it was recently shown that most LLCPs at one month of age in mice are marked by expression of GLI-Kruppel family member 1 (*Gli1*)[13]. Since *Gli1* is also expressed in the fetal limb[14], it is unclear whether a subpopulation of Gli1$^+$ cells acquire this potential intrinsically with time (Suppl. Fig. 1.i), or due to microenvironmental changes from the SOC or perichondrium (Suppl. Fig. 1.ii-a and -b), or whether they always have this potential but remain dormant until previous progenitors have been used up (Suppl. Fig. 1.iii). Moreover, it is not known whether the LLCPs are located in the cartilage anlagen since they are formed (Suppl. Fig. 1.iii-a), or whether they derive from stromal precursors (either Gli1$^+$ or Gli1$^-$) that contribute to Gli1$^+$ CPs at later stages (Suppl. Fig. 1.iii-b).

In this study, we show that a majority of LLCPs derive from fetal Gli1$^+$ cells. Some of these Gli1$^+$ cells are already present in the early cartilage (but remain quiescent until the third postnatal week) while others are seeded progressively from the surrounding tissues. Moreover, these Gli1$^+$ progenitors can be generated *de novo* from cells of the Pdgfra lineage in response to cartilage cell-cycle arrest, revealing a heretofore unknown plasticity of the fetal limb. We posit that this fundamental knowledge will be critical to understanding and manipulating cartilage growth and repair.

Main text

Fetal Gli1$^+$ cells give rise to most chondrocyte long columns in the juvenile and adult growth plate

When Gli1$^+$ cells are lineage-traced at P30, they label ~70% of chondrocytes of the growth plate one month later[13]. Since Gli1$^+$ cells exist in the limb from fetal stages, both inside and outside the cartilage (Suppl. Fig. 2a), we set out to determine whether fetal Gli1$^+$ cells already contain LLCPs. We crossed mice bearing a tamoxifen-inducible CreER^{T2} targeted into the *Gli1* locus[14] (*Gli1*^{CreER} hereafter) with reporter mice containing lox-STOP-lox-tdTomato in the *Rosa26* locus (*R26*$^{LSL\text{-}tdTom}$ hereafter, Fig. 1a)[15]. We provided tamoxifen (TM) at either E12.5 or E13.5 and quantified the number of tdTom$^+$ cells at multiple stages (E14.5, 17.5, 19.5, P30 and 60). In all cases, tdTom$^+$ cells were found both inside the cartilage and adjacent tissues: interzone knee region, perichondrium, metaphysis and secondary ossification centres (Fig. 1a, a'). Since fetal CPs do not self-renew[2], we expected the % of labelled chondrocytes to decrease with time. In contrast, the contribution of Gli1-lineage cells to cartilage rather increased with time, labelling 65-70% of chondrocytes in the 2-month-old growth plate (Fig. 1b). To determine when in this process Gli1-derived chondrocytes switched from forming short to forming long clonal columns, we used a reporter line (RGBow, Fig. 1c)[16] whereby one membrane-bound fluorescent protein (out of three potential ones) is randomly expressed via Cre-recombination. After giving TM at E12.5 or 13.5, we analysed the number, length and location of distinct columns in the three zones of the cartilage. Notably, the total number of columns increased up to P0-P1, the majority located in the RZ and PZ (Fig. 1c) and composed of 2-3 cells (Fig. 1d). By P14, the total number of columns was greatly reduced but their length started to increase (Fig. 1d). By P30, few columns remained, but they ran along the whole growth plate, starting from the RZ (Fig. 1c, d). In short, the results indicated that Gli1$^+$ cells at E12.5-13.5 give rise to CPs with two different fates: short-lived, that get depleted over time, and long-lived ones that remain dormant at perinatal stages but become active after ~P14.

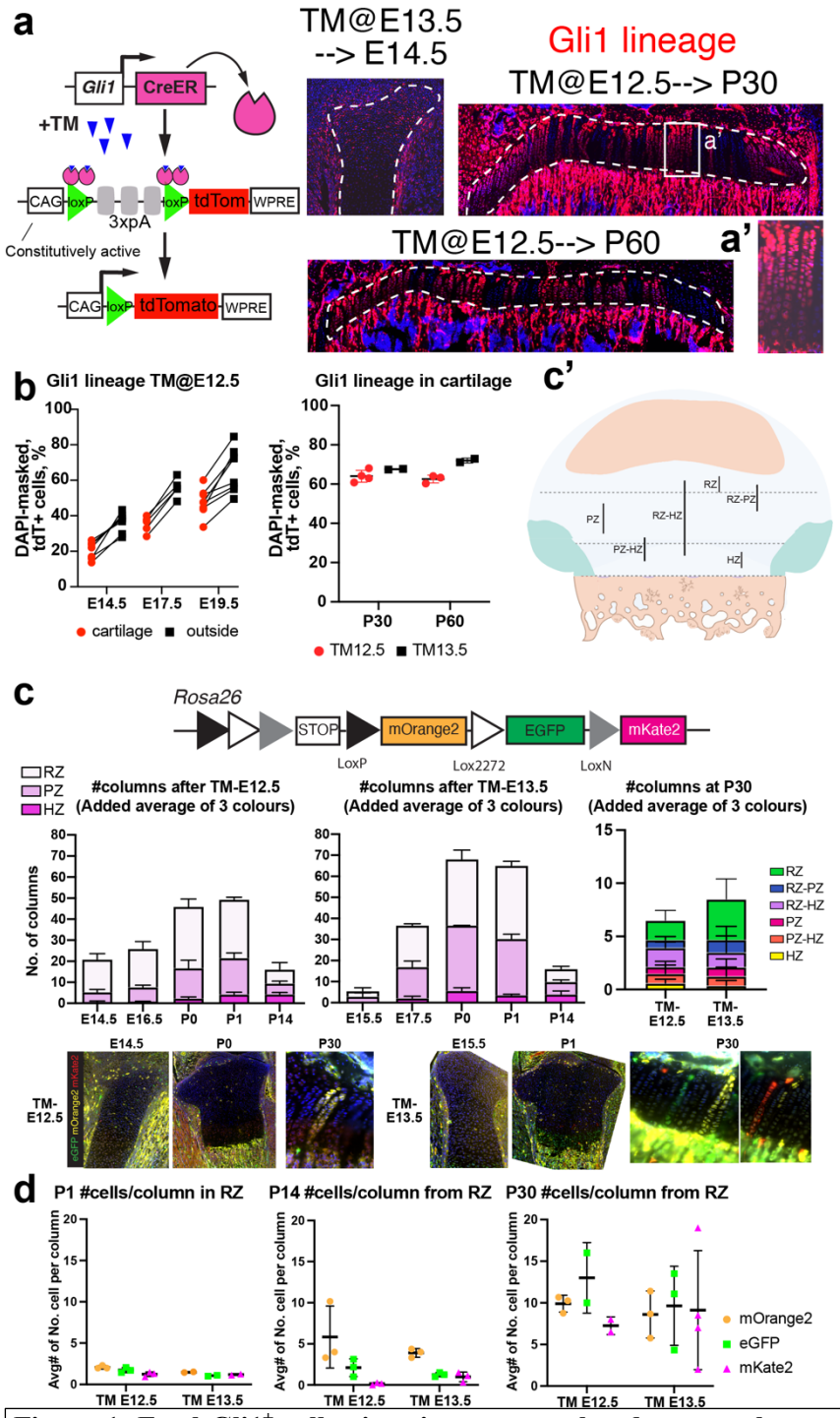

Figure 1. Fetal Gli1$^+$ cells give rise to most chondrocyte columns in the juvenile & adult growth plate. a Lineage tracing of Gli1$^+$ cells after tamoxifen (TM) induction at embryonic stage (E) 12.5 or 13.5, analysed at the indicated stages. **b** Quantification of reporter-expressing cells, inside and outside the cartilage for E12.5 injection (left), or in cartilage for both induction times (right). **c-c'** Tri-colour reporter RGBow (c) was used to quantify individual clones in the growth plate (added average of each colour shown), at multiple times post induction. RZ, PZ, HZ: resting, proliferative, hypertrophic zone. c', Schematic of zone-crossing clones. **d** # of cells per RZ-rooted column.

LLCPs are derived from Gli1$^+$ cells that progressively populate the fetal and perinatal cartilage

We next asked whether Gli1-derived LLCPs were already present in the early cartilage (~E12.5), and/or seeded later from the adjacent tissues (the latter suggested by studies showing that chicken perichondrium is a reservoir for cartilage precursors[17]). We generated a mouse line whereby expression of nuclear Green Lantern is controlled by a tetracycline-response-element, targeted into the Tightly regulated locus (*Tigre* or *Igs7*) (Suppl. Fig. 3a-b and Fig. 2a, *Tigre*$^{TRE\text{-}nGL}$ hereafter). We then crossed *Gli1*$^{CreER/CreER}$; *Tigre*$^{TRE\text{-}nGL/TRE\text{-}nGL}$ females with *Col2a1-rtTA/+*[18]; *R26*$^{LSL\text{-}tdTom/LSL\text{-}tdTom}$ males, and provided TM at E13.5 to label the Gli1-lineage with tdTom, and a 24-h pulse of Dox (either at E12.5 or E17.5) to transiently express nGL in fetal chondrocytes (Suppl. Fig. 3c). We then followed the green signal over time, with the expectation that quiescent cells (i.e. LLCPs) would retain fluorescence for longer than cells dividing quickly. By providing Dox at different points, we aimed to label two potential CP populations: those already resident in the early cartilage anlage (Fig. 2a.i), and those seeded later into the cartilage (Fig. 2a.ii). As expected, most green cells after E12.5-Dox were found inside the cartilage (only 2-4% of perichondrial cells were GL$^+$ at E14.5, Suppl. Fig. 3c-c'; while 40-50% of cells in cartilage were GL$^+$ at E17.5, Fig. 2b-b'). The number of GL$^+$ chondrocytes dropped fast (less than 20% were GL$^+$ at E19.5, Fig. 2b'), stabilising at 1-2.5% in the P14-P21 RZ and becoming undetectable from P21 to P30 (Fig. 2b'). Most GL$^+$ cells were negative for the proliferative marker Ki67 at all stages analysed (Supp. Fig. 3d), supporting the notion that they were quiescent. Of note, the % of Gli1-lineage chondrocytes within the GL$^+$ population increased over time, until 100% of label-retaining CPs in the P21 RZ belonged to the E13.5-labelled Gli1-lineage (Fig. 2c). Conversely, <5% of Gli1-lineage cells in the P21 RZ were GL$^+$, indicating that the Gli1-lineage contains other subpopulations (Fig. 2d). Similar results were obtained when Dox was given at E17.5 (Fig. 2b''), except for the % of GL$^+$ cells in the Gli1-lineage of the RZ cartilage. After E12.5-Dox, this measure stabilised at 2-5% by P14, while after E17.5-Dox, it reached up to 10% by P14 and P21, only dropping at P30 (Fig. 2d-f). Of note, P14 and P30 GL$^+$tdT$^+$ cells were exclusively found in the upper layers of the RZ, adjacent to the secondary ossification centre (SOC, Fig. 2g). These results suggested that while some LLCPs are already present in the fetal cartilage (Fig. 2a.i), new LLCPs are also added at least until birth, derived from fetal Gli1$^+$ stromal cells (Fig. 2a.ii).

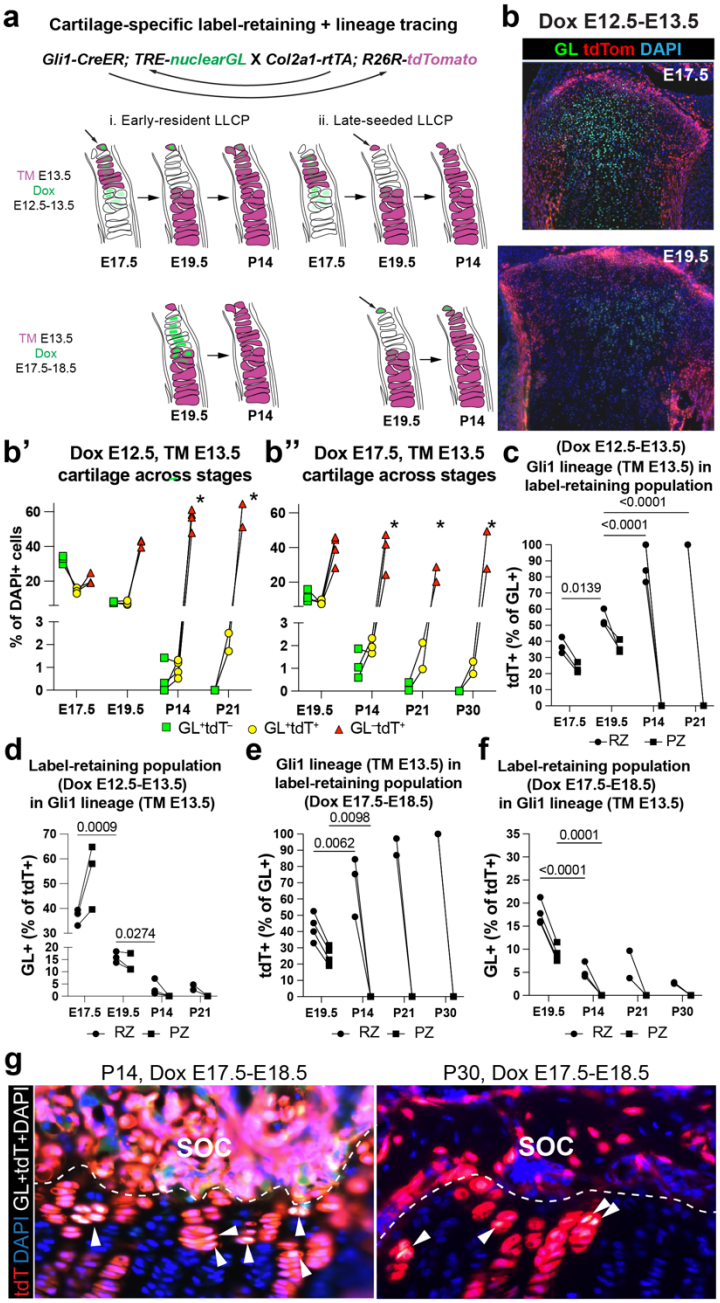

Figure 2: Gli1-derived LLCPs populate fetal & perinatal cartilage. a Model to label the Gli1 lineage and label-retaining chondrocytes, and the expected results of early and late Dox induction for two scenarios: LLCPs are present in the early cartilage (i) or seeded later (ii). **b-b''** Typical images at E17.5 and E19.5 (b) and quantification of single-positive and double-positive populations in the cartilage at the indicated stages when Dox was given at E12.5 (b') or E17.5 (b''). *: P14, P21 quantified in resting zone (RZ) only. **c-f** % of tdT$^+$ cells within the GL$^+$ population (c, e) or vice versa (d, f) after 1-d Dox pulse at E12.5 (c, d) or E17.5 (e,f). p-values for Sidak's multiple comparisons test after 2-way ANOVA are shown. **g** Proximal tibia after 1-d Dox pulse at E17.5. Arrowheads, GL$^+$tdT$^+$ nuclei. Dashed lines separate the RZ and the secondary ossification centre (SOC).

Chondrocytes generated in the last postnatal week from Gli1⁺ cells are required for long-term bone growth

To test if Gli1-derived chondrocytes are required to sustain bone growth, we used a *Tigre*$^{Dragon\text{-}aDTA}$ allele[19,20] in which inducible expression of attenuated diphtheria toxin (aDTA) requires Cre and rtTA activity (Fig. 3a). We crossed *Gli1*^{CreER}; *Tigre*$^{Dragon\text{-}aDTA}$ mice with *Col2a1-rtTA; R26*$^{LSL\text{-}tdTom}$, and gave TM at E13.5 and Dox E12.5-P0. This way, only chondrocytes were ablated among Gli1-descendants (Fig. 3a, b-b'). While the ablation was incomplete and only sustained for a short time, this targeted injury led to reduced bone length by P100, especially for the tibia (Fig. 3c). This revealed the important role of fetal/perinatal Gli1-derived chondrocytes in long-term bone growth. Of note, ablation could not be sustained postnatally due to insufficient sensitivity of *Col2a1-rtTA* to Dox (Suppl. Fig. 4), raising the possibility that partial compensation had taken place postnatally (see Discussion).

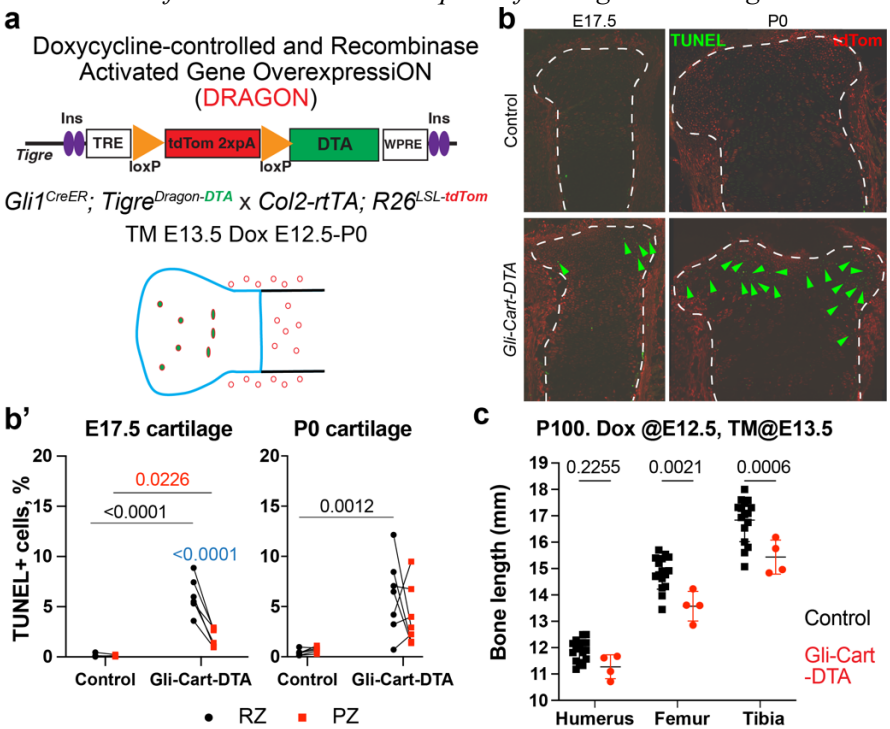

Figure 3. a The Dragon-DTA allele described in refs. [19-20] was combined with *Gli1*^{CreER} and *Col2a1-rtTA* to activate diptheria toxin expression exclusively in Gli1-lineage chondrocytes in the last week of gestation (*Gli-Cart-DTA* model). **b-b'** Typical images (b) and quantification (b') of TUNEL⁺ cells at the indicated stages. **c** Bone length of Ctl and *Gli-Cart-DTA* mice at postnatal day 100 (P100). In b' and c, p-values of multiple comparisons tests after 2-way ANOVA are shown.

Mosaic cell-cycle arrest in the fetal cartilage triggers compensation from Gli1⁺ cells

Since Gli1⁺ cells have been shown to participate in the repair of bone fractures[21], we next asked whether fetal Gli1⁺ cells participate in the compensation of cartilage growth challenges. We previously showed that left-limb-cartilage-specific, salt-and-pepper expression of p21/CDKN1A–a CDK1 inhibitor that blocks the G1-S transition[22]–is compensated by hyperproliferation of spared cells in fetal mice[23] (*Left-Cart-p21* model hereafter). To investigate the origin of the compensating cells, we undertook an unbiased single-nuclei RNA-seq approach of left and right fetal knees from two E16.5 control (Ctl) and two *Left-Cart-p21* embryos (ExpL and ExpR, Fig. 4a and Suppl. Fig. 5a). Out of the original dataset (~32,000 nuclei in 32 clusters, Suppl. Fig. 5b), which contained mostly lateral plate mesoderm (LPM)-derived cells, and a minority of muscle and endothelial cells, we further explored the LPM subset (21,000 nuclei, Fig. 4a'). This subset was composed of 23 clusters (Suppl. Fig. 5c, d), which we grouped in five main categories: chondrocytes, tenocytes, fibroblasts, perichondrium and joint-associated mesenchymal cells. The Propeller tool[24] revealed that, within Gli1^{high} cells, the proportion of cells belonging to the chondrocyte group was increased in experimental limbs, as compared to Ctl (Fig. 4a''). Of note, this change in proportions was not observed in other populations, such as Pdgfra^{high} cells (Suppl. Fig. 5e).

To confirm these findings, we turned to Cre-based lineage tracing. To trace the Gli1-lineage independently of p21 expression, we utilised a Cre-independent p21-expression system, targeted to cartilage elements (*Col2a1-rtTA; Tigre*$^{TRE\text{-}p21}$, *Cart-p21* hereafter)[19]. *Gli1*$^{CreER/CreER}$ females were crossed with *Cart-p21; R26*$^{LSL\text{-}tdTom/LSL\text{-}tdTom}$ males and given Dox at E12.5 and TM at E13.5. (Fig. 4b). As with the left-limb-targeted model, we confirmed that expression of p21 in 60-70% of chondrocytes (Suppl. Fig. 6a) did not cause growth defects by P0 (Fig. 4b'). Interestingly, despite continuous Dox exposure, the fraction of p21⁺ chondrocytes decreased with time (Suppl. Fig. 6a), as we previously described with the *Left-Cart-p21* model[23]. To assess the involvement of Gli1⁺ cells in this compensatory response, we followed tdTom⁺ distribution inside and outside the cartilage 1, 4 and 7 days post TM (dpt, Fig. 4c, c'). In *Cart-p21* mice, the Gli1-lineage showed a significant expansion in the cartilage, as compared to controls, at all stages analysed (Fig. 4c'). These results suggested that, in controls mice, some E13.5-

Gli1-derived chondrocytes only contribute transiently and are then "pushed out" of the cartilage, while in *Cart-p21* limbs, the Gli1-lineage increases its contribution to longer-lived CPs. Moreover, the contribution outside the cartilage also seemed expanded in P0 *Cart-p21* limbs compared to controls (Fig. 4c'), suggesting the p21^{+} cartilage signals to adjacent tissues. Since CPs reside in the resting zone, we split the cartilage analysis into resting and proliferative zones (RZ and PZ). Both showed enhanced contribution of the Gli1-lineage, typically biased towards RZ (Suppl. Fig. 6b-d).

To test the role of Gli1-lineage chondrocytes in the compensation of cartilage-targeted p21 activity, we combined *Cart-p21* and *Gli1-Cart-DTA* models. We expected many of the Gli1-lineage chondrocytes newly generated upon cartilage-targeted p21 expression to express DTA, hindering their reparative role (Fig. 4d). After E12.5-Dox and E13.5-TM, the proportion of TUNEL^{+} chondrocytes at E17.5 and P0 showed an upwards trend in *Cart-p21; Gli1-Cart-DTA* as compared to *Gli1-Cart-DTA* mice (Fig. 4d), despite not reaching significance. Bone length was reduced in P0 *Cart-p21; Gli1-Cart-DTA* mice as compared to controls and/or *Cart-p21* mice, indicating that Gli1-derived chondrocytes are required for the compensation of cartilage-targeted p21, even as early as P0 (Fig. 4d'). Due to increased mortality of *Cart-p21; Gli1-Cart-DTA* mice, we were not able to analyse later time points.

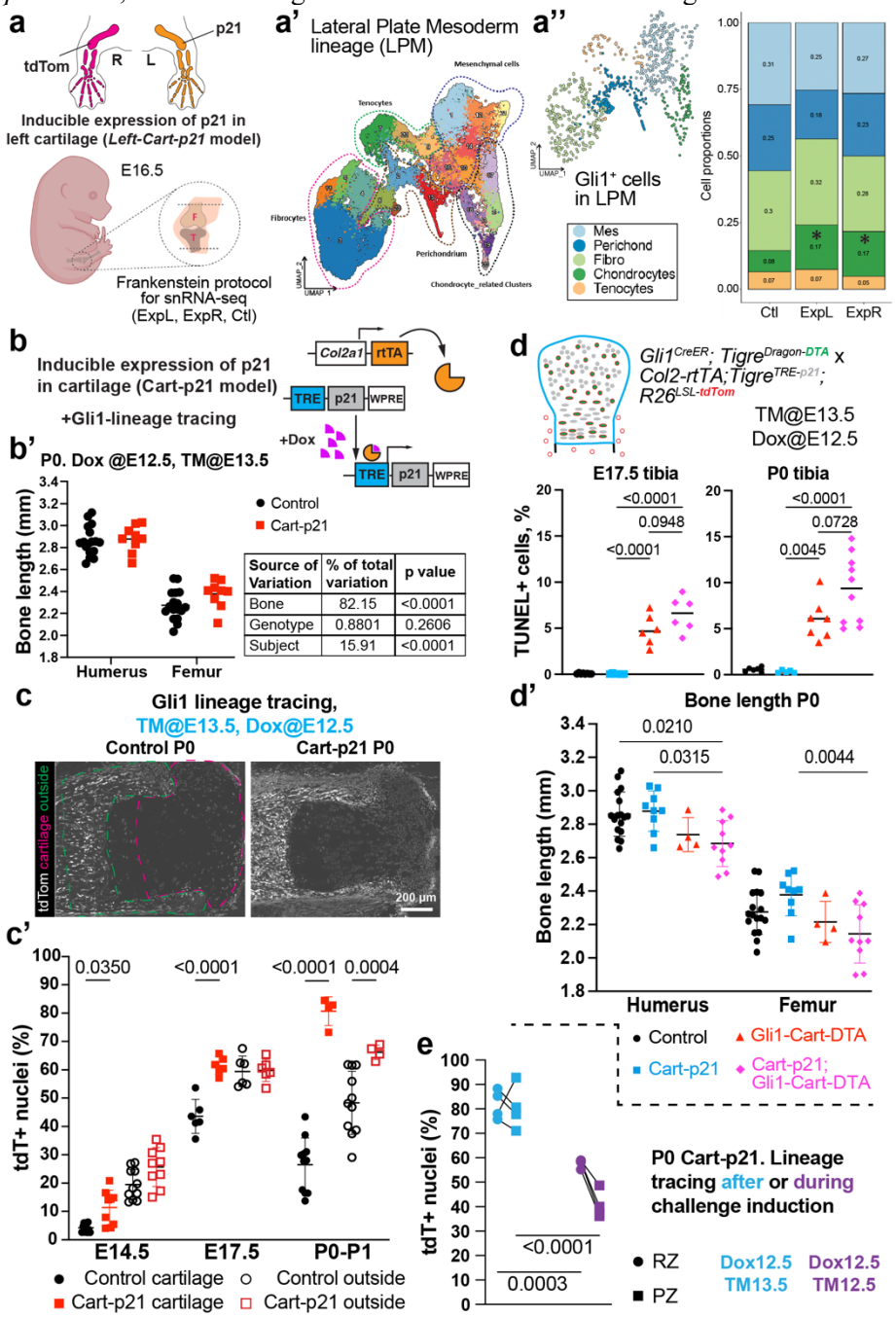

Figure 4. Mosaic cell-cycle arrest in the fetal cartilage triggers compensation from Gli1^{+} mesenchymal cells. a-a'' A left-cartilage targeted model of p21 overexpression (*Left-Cart-p21*) was used for single-nuclei RNA-seq analysis of knees. Left and right knees from 2 embryos per genotype (rtTA^{+} and $^{-}$) were processed separately, but left and right cells from control embryos were analysed together, as control group (a). The cells derived from lateral plate mesoderm (LPM) were further subclustered (a') and then filtered by Gli1 expression so that the proportion of each cell type could be compared across genotypes (a''). **b-b'** Expression of p21 in the cartilage, induced from E12.5 to P0 (b), does not lead to growth defects (b'). **c-c'** The Gli1 lineage was followed in the absence (Control) and presence of p21 misexpression in the cartilage (*Cart-p21*), and quantified inside and outside the cartilage (defined in c). In c', p-values for multiple comparisons test after 2-way ANOVA are shown. **d-d'** Schematic of the genetic approach to induce p21 expression in the cartilage, recruiting Gli1^{+} cells, while inducing DTA expression in Gli1-derived chondrocytes, to interfere with their reparative role. For all genetic combinations, apoptotic cells were detected by TUNEL (d) and bone length measured at P0 by micro-CT (d'). **e** Comparison, in *Cart-p21* P0 samples, of tdT distribution upon two induction regimens.

Pdgfra$^+$ cells outside the cartilage become Gli1$^+$ chondrocytes upon cell-cycle arrest in the cartilage

We next set out to determine the source of the additional Gli1$^+$ cells upon p21 misexpression. Since our initial labelling of the Gli1-lineage was done one day after the induction of p21 expression, we were not able to distinguish between expansion of the existing Gli1$^+$ population vs. *de novo* expression of *Gli1* in cells that were Gli1$^-$ before. To explore this possibility, we inverted the induction order when following Gli1-lineage in the *Cart-p21* model (Suppl. Fig. 6b). The Gli1-lineage showed a similar trend in the TM-E12.5 control cartilage as compared to TM-E13.5, although a few more descendants were found outside the cartilage by P0 (Suppl. Fig. 6b, compare with Fig. 4c'). However, in *Cart-p21* limbs, the Gli1-lineage increased its contribution to cartilage at a slower pace in E12.5-TM/E13.5-Dox litters as compared to E13.5-TM/E12.5-Dox (Fig. 4c', Suppl. Fig. 6b, note E17.5), only becoming significantly higher than in controls by 7 dpt (see Suppl. Fig. 6c-d for a division into RZ and PZ). However, in E13.5-Dox samples, the fraction of p21$^+$ chondrocytes remained quite constant across stages (Suppl. Fig. 6a'), as opposed to the progressive decrease observed in E12.5-Dox samples (Suppl. Fig. 6a). Therefore, to compare behaviours under identical compensatory conditions, we also analysed a third regimen: E12.5-TM/E12.5-Dox, finding that the number of descendants was lower in P0 *Cart-p21* as compared to E13.5-TM/E12.5-Dox (Fig. 4e, Suppl. Fig. 6c'', d').

Collectively, these results suggest that while the existing population of Gli1$^+$ cells can contribute to some extent to the repair, some Gli1$^-$ cells become Gli1$^+$ <u>after</u> *p21* induction in the cartilage. To further explore this possibility, we performed pulse-chase experiments with the thymidine analogue 5'-ethynyl-2-deoxyuridine (EdU). EdU was injected once at either E14.5 or E15.5, and chased up to E17.5 (Suppl. Fig. 7a). In both cases, while there was an obvious decrease in the number of EdU$^+$ chondrocytes in *Cart-p21* embryos as compared to control ones (Suppl. Fig. 7b,c), there were still more than expected, given that >60% chondrocytes express p21 in this model (Suppl. Fig. 6a), and that most p21$^+$ chondrocytes cannot incorporate EdU (Fig. 1G in ref.[23]). Interestingly, however, more than one third of EdU$^+$ chondrocytes were also p21$^+$ (Suppl. Fig. 7b', c') and, conversely, many p21$^+$ RZ chondrocytes were EdU$^+$ in *Cart-p21* mice, especially after E14.5-EdU (Suppl. Fig. 7b'', c''), compared to very low numbers in controls. This could be explained by two non-exclusive scenarios: 1) some p21$^-$ chondrocytes incorporate EdU, and then become p21$^+$; 2) p21$^-$ cells from outside the cartilage incorporate EdU, and then migrate to the cartilage, becoming *Col2a1-rtTA*$^+$ (and thus p21$^+$) chondrocytes. Since the number of p21$^+$ chondrocytes did not increase, but rather decrease, over time (Suppl. Fig. 6a), the first scenario was deemed unlikely, suggesting the possibility that most EdU$^+$ p21$^+$ chondrocytes derive from cells located outside the cartilage (Suppl. Fig. 7d).

Along these lines, we next investigated the relationship between Gli1$^+$ cells and other populations outside the cartilage in the snRNA-seq dataset (E16.5). Within the 945 Gli1^{high} cells, we found that the proportion of Pdgfra$^+$ cells in multiple mesenchymal cells was decreased in the ExpL samples, as compared to ExpR and Ctl (Fig. 5a). Moreover, the chondrocyte population was specifically increased in the Pdgfra^{low}Gli1^{high} LPM population of ExpL and ExpR limbs, as compared to Ctl (Fig. 5b). Within chondrocytes, velocity analyses suggested that *Gli1* was upregulated in the osteochondroprogenitors (OCPs) of ExpL limbs, and that these cells increased their contribution to resting and proliferative chondrocytes (Fig. 5c). Thus, we posited that Pdgfra^{high} cells, which normally surround the E14.5 cartilage (Suppl. Fig. 2b), become Gli1^{high}Pdgfra^{low}, and migrate to the cartilage in response to cartilage-p21. To confirm this possibility, we performed a single-cell RNA-seq experiment of *Cart-p21* limbs at an earlier time point (E14.5), separating between Gli1-lineage and non-Gli1-lineage cells (Suppl. Fig. 8a-e, Fig. 5d-d'). RNA velocity analysis suggested that, within the non-Gli1-lineage, *Pdgfra* expression was being downregulated in the experimental perichondrium (Fig. 5d''). Moreover, the proportion of perichondrial cells within the Gli1^{high}Pdgfra^{low} population was decreased (while the proportion of resting chondrocytes increased) in Exp Gli1-lineage samples vs. control Gli1-lineage samples (Fig. 5e), which is compatible with the relocation from the perichondrium to the resting zone in response to *Cart-p21*. To capture the potential arising of new Gli1$^+$ cells within the Pdgfra-lineage, we crossed *Pdgfra*$^{CreER/+}$ females with *Cart-p21*; *R26*$^{LSL\text{-}tdT/LSL\text{-}tdT}$ males and provided E12.5-Dox and E13.5-TM (Fig. 5f). We then compared the overlap of Pdgfra-lineage and *Gli1*$^+$ cells between *Cart-p21* and control samples. In the E17.5 *Cart-p21* cartilage, the number of *Gli1*$^+$ cells was significantly increased, as compared to controls, within both the Pdgfra-lineage and the total cartilage (Fig. 5f'). The overall contribution of the Pdgfra-lineage to cartilage was not increased at E17.5 (Fig. 5f', sum of white and green), although it was mildly increased at P0 (Suppl. Fig. 9a). This confirmed the hypothesis that some Pdgfra$^+$

cells become Gli1$^+$ in response to *Cart-p21*, contributing to compensation. Of note, the Pdgfra-lineage showed persistent hyperproliferation in the *Cart-p21* RZ between E14.5 and E17.5, as opposed to the non-Pdgfra lineages (Suppl. Fig. 9b-c'), but did not show this behaviour outside the cartilage. Given that at P1 almost no Pdgfra$^+$ cells could be found within the cartilage (Suppl. Fig. 2b') these results suggested that some Pdgfra$^+$ cells located in the perichondrium downregulate *Pdgfra* expression and contribute to cartilage in normal conditions, but that most of them do not give raise to Gli1$^+$ LLCPs unless the cartilage is challenged (Fig. 5g). This was confirmed by long-term Pdgfra-lineage tracing with the RGBow reporter giving rise to very few long columns in P30 control mice, most of them restricted to the growth plate periphery and the perichondrium (Suppl. Fig. 9d-e).

Discussion

Elucidating the origin and regulation of the LLCPs is crucial to understanding the evolution of limb size and proportions, the factors that influence human height and the potential causes and treatments of skeletal dysplasias. Major advances have been recently made in the field, especially in mouse models, identifying cell populations in postnatal cartilage that can self-renew and give rise to

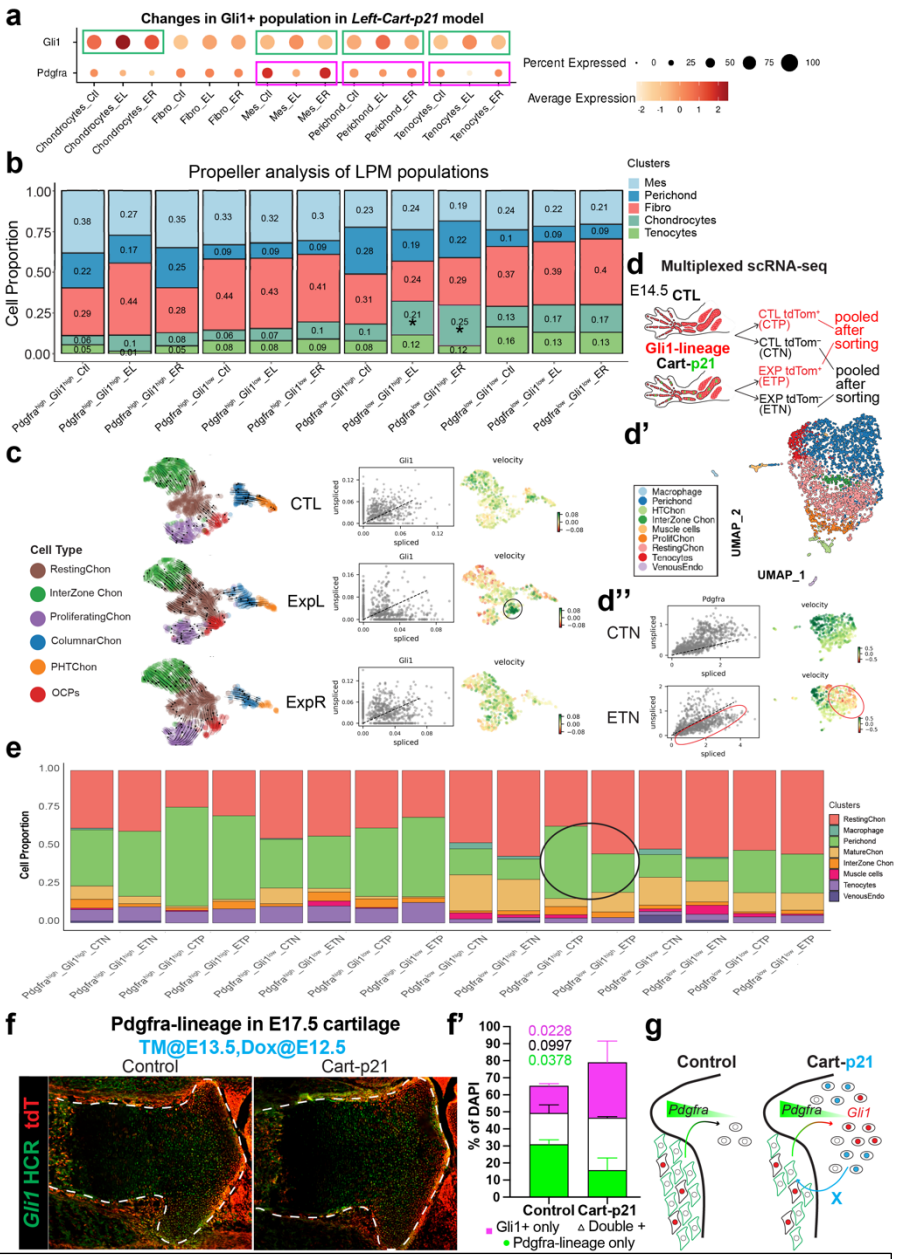

Figure 5. *Pdgfra*$^+$ cells outside cartilage become Gli1$^+$ chondrocytes upon cell-cycle arrest in the cartilage. **a** DotPlot within the Gli1$^+$ population in the mesenchyme of E16.5 Ctl and *Left-Cart-p21* limbs shows that *Pdgfra* expression (levels and number of expressing cells) are decreased in various ExpL mesenchymal populations (magenta rectangles), which correlates with increased levels of *Gli1* expression in those populations and chondrocytes (green rectangles). **b** Comparison of cell-type proportions (indicated by numbers inside the bars) across experimental conditions, divided according to *Pdgfra* and *Gli1* expression. Asterisks denote significant difference, as calculated by Propeller. **c** Left: Pseudotime analysis of Ctl and *Left-Cart-p21* mesenchymal cells using scvelo. Note the potential contribution of ExpL osteochondroprogenitors (OCPs) to resting and proliferative chondrocytes. Right: RNAvelocity analysis of the same samples, predicting upregulation of *Gli1* in OCPs (black oval). **d-d''** New single-cell RNA-seq from E14.5 hindlimbs (Ctl and *Cart-p21*), separating Gli1-lineage and non-lineage cells (d), resulting UMAP and cell clusters (d') and RNAvelocity predicting *Pdgfra* downregulation in perichondrium (d'', red oval). **e** Propeller analysis of cell-type proportions across experimental conditions, divided according to *Pdgfra* and *Gli1* expression. Note the perichondrial depletion within the Pdgfra^{low}Gli1^{high} in Exp Gli1-lineage (oval). **f-f'** Tracing of Pdgfra lineage (tdT) and *Gli1* hybridisation chain reaction (HCR) in E17.5 Ctl and *Cart-p21*, as indicated (f), and quantification of single- and double-positive populations (f'). **g** Model of the contribution of perichondrial Pdgfra$^+$ cells to Gli1$^+$ chondrocytes in response to X signal from *Cart-p21* cartilage.

long columns of chondrocytes for most or all of the growth period[8,9,13]. However, given that at fetal and perinatal stages only short columns are generated[2], it is unclear whether the LLCPs are already present in the early cartilage and, if so, whether they are a separate population that switches behaviour due to intrinsic and/or extrinsic factors, or rather are equivalent to all other CPs, but are spared from the depletion of early stages because of their initial location, further from the proliferative zone. In this work, we show that fetal Gli1$^+$ mesenchymal cells give rise to LLCPs, as the Gli1-lineage labelled at E12.5-E13.5 makes up most of the chondrocytes at P30 and P60 (Fig. 1). Moreover, we showed that while the E12.5-E13.5 cartilage already contains some Gli1$^+$ label-retaining CPs, the E17.5-E18.5 cartilage contains a higher proportion of Gli1-lineage chondrocytes that are label-retaining (Fig. 2), suggesting that new waves of LLCPs are added from outside the cartilage, at least in the last gestational week. The fact that not all Gli1$^+$ cells were label-retaining at these stages (Fig. 2), implied either that there are subpopulations within Gli1-lineage cells, or that they are all identical but allocated to different fates depending on their initial location (i.e. cells located in the upper layers of the RZ are less likely to be recruited to the PZ during perinatal stages) and/or stochastic variation. Importantly, our single-nuclei/single-cell RNA-seq analyses did not identify overly different subpopulations within Gli1-lineage chondrocytes, supporting the scenario that all Gli1$^+$ CPs are equivalent. Of note, for this analysis Gli1-lineage cells had to be FACS-separated instead of bioinformatically identified, because the 10x approach is 3' biased, such that both the tdTom and the p21 transgenes yield reads mapping to WPRE, the RNA-stabilising sequence used in both cases (Fig. 1a and 4b).

Given the role of adult Gli1$^+$ osteoprogenitors in fracture repair[21], we used our Cre- and rtTA-dependent strategy to ablate only the chondrocytes within the E13.5-Gli1 lineage, and only during the fetal period (Dox E12.5 to P0) to test their role in normal growth (Fig. 3). While bone length was significantly affected, the effect was somewhat mild. This was probably due to compensation after Dox clearance. While we tried to test this possibility by providing Dox postnatally, the rtTA that we used in our models did not get sufficiently activated (Suppl. Fig. 4).

Following up on the role of Gli1-derived chondrocytes, our single-nuclei/single-cell RNA-seq analyses suggested that these cells contributed to the compensation of p21 misexpression in the cartilage, which we confirmed via lineage tracing (Fig. 4). The ablation of Gli1-derived chondrocytes during the compensation of cartilage cell cycle arrest led to a significant but mild growth reduction by P0 (Fig. 4). The effect would have been presumably larger at later stages, but these could not be analysed, because quadruple transgenic animals did not survive long.

As previously introduced, an outstanding question in the field is whether the fetal precursors of the LLCPs are all located in the cartilage, or whether some of them are located in the surrounding tissues and ingress in the cartilage later. Since our *Col2a1-rtTA* pulsed at E12.5 labels virtually only cartilage cells (Suppl. Fig. 3), our data indicates that the E12.5 cartilage anlage already contains a significant amount of Gli1$^+$, quiescent LLCPs (Fig. 2). However, it also suggests, that Gli1$^+$ cells outside the initial cartilage anlagen likely contribute to the LLCP pool later, as an E17.5-E18.5 Dox pulse led to a higher proportion of Gli1-lineage cells retaining the Col2a1-rtTA activated nuclear label (Fig. 2). This behaviour is likely exacerbated in response to growth challenges in the cartilage. Indeed, changes in the Dox/TM administration order and EdU pulse-chase experiments in the *Cart-p21* model (Suppl. Figs. 6 and 7) suggested that Gli1$^-$ cells located outside the cartilage become Gli1$^+$ and participate in the compensatory response. In this regard, the bioinformatics analysis suggested that perichondrial Pdgfra$^+$ cells become Gli1$^+$ and then become incorporated in the cartilage, which was supported by our Pdgfra-lineage tracing experiments (Fig. 5). A question for future studies is which signals are produced by the *Cart-p21* cartilage that recruit Pdgfra-lineage cells (signal X in Fig. 5g). Of note, perichondrial Pdgfra$^+$ cells do not seem to contribute many LLCPs in control conditions (Suppl. Fig. 9), raising another future question: are there other perichondrial cells that contribute to LLCPs during normal growth?

Lastly, an interesting observation from our unilateral model (*Left-Cart-p21*) is that sometimes the ExpR limb (internal control) showed a similar response to the ExpL one (Fig. 4a'', 5b). The fact that other responses were detected exclusively in the ExpL limb (Fig. 5c) strongly suggests that the responses of the ExpR limb are not merely a consequence of low-level activation of p21 on the right cartilage, but rather due to a systemic effect triggered by inter-organ communication. It is worth noting that we have previously reported a similar effect on distant cartilage (limb and ribs) upon left-cartilage specific expression of p21 and DTA[20,23]. Moreover, systemic mediators of local tissue repair and regeneration have been shown in multiple species[25]. While fully investigating this phenomenon is beyond the scope of this study, we posit that inter-organ communication primes distant tissues to respond to challenges, but that the full response also requires local cues only present in the injured tissues. Our unilateral injury models will be powerful tools to elucidate this process.

Methods

Animal models

The use of animals in this study was approved by the Monash Animal Research Platform animal ethics committee at Monash University (protocol 32263).

Unilateral p21 expression model: The *Pitx2-ASE-Cre* (aka *Pitx2-Cre*) mouse line, obtained from Prof. Hamada[26], was crossed with the *Col2a1-rtTA* mouse line[18], and then inter-crossed to generate *Pitx2-Cre/Cre; Col2a1-rtTA* mice. In some experiments, a *Col2a1-eCFP* allele[27] was also included (a kind gift from David Rowe). Genotyping was performed as described previously[23]. The $Tigre^{Dragon\text{-}p21}$ mouse line was previously described[19,23]. Experimental and control animals were generated by crossing *Pitx2-Cre/Cre; Col2a1-rtTA/+* females with $Tigre^{Dragon\text{-}p21/Dragon\text{-}p21}$ males (i.e. homozygous for the conditional misexpression allele). The separation of control and experimental animals was based on the rtTA genotype. Pregnant females were administered doxycycline hyclate (Sigma) in water (1 mg/kg with 0.5% sucrose) from E12.5 until collection (or until birth). The day of vaginal plug detection was designated as E0.5, and E19.5 was referred to as P0.

Postnatal *Col2a1-rtTA* induction tests: Experimental and control animals were produced by crossing *Pitx2-Cre/Cre; Col2a1-rtTA/+* females with $Tigre^{Dragon\text{-}DTA/Dragon\text{-}DTA}$ males. Pups were administered doxycycline hyclate (Sigma, 1 mg/ml in drinking water, with 0.5% sucrose for palatability) and food (600 mg/kg, SF08-026 from Specialty Feeds) from P15.5 to P18.5, followed by tissue collection at P18.5.

Lineage tracing combined with p21 expression in all cartilage elements: $Gli1^{CreER/CreER}$ females[28] were crossed with *Col2a1-rtTA/+;* $Tigre^{TRE\text{-}p21/TRE\text{-}p21}$*;* $R26^{LSL\text{-}tdT/LSL\text{-}tdT}$ males (described in [15,19]). Pregnant females were given doxycycline in food (600 mg/kg, SF08-026 from Specialty Feeds) and in water (as described above), plus tamoxifen (180 µg/g via oral gavage), at the stages described in the main text. To trace other lineages, $Pdgfra^{CreER}$ females[29] (a kind gift from Brigid Hogan) were used instead of $Gli1^{CreER}$ ones (100 µg/g tamoxifen via oral gavage). $Pdgfra^{H2B\text{-}EGFP}$ mice[30] (aka $Pdgfra^{GFP}$) were a gift from Philippe Soriano.

Generation of G4 mouse embryonic stem cells with Tigre docking site*:* a TIGRE docking site targeting vector (a gift from Hongkui Zeng via Addgene plasmid #61580; http://n2t.net/addgene:61580; RRID:Addgene_61580) was electroporated by Monash Genome Modification Platform into G4 mESCs (a gift from Andras Nagy) to generate an ESC line (MG36) with a docking site in the *Tigre* (*Igs7*) locus, amenable for Flp-mediated cassette exchange. 192 individual clones were picked after 6 days of G418 selection. Out of the 96 analysed clones, 21 were positive by Southern hybridisation with both 5' and 3' probes. After reanimation, these clones were analysed again by Southern hybridisation, 8 positive clones were further characterised by Southern hybridisation using internal neo probe (3 restriction digestions); 7 clones (#9, 13, 17, 32, 56, 61, 62) showed single integration. After sequencing, all positive clones were found to have the correct sequence at F5 and F3 mutant FRT sites. 4 clones were karyotyped: clones #56 and 62 are 100% euploid metaphase, whereas clone #32 was 87% euploid, and clone #9 80% euploid.

Generation of $Tigre^{TRE\text{-}nucGreenLantern}$: AR157 vector, containing a TRE-H2B-GreenLantern and a PGK-Hygro resistance split gene (N-half) flanked by FRT sites was generated by VectorBuilder (Suppl. Fig. 3a). The vector also contained a Polylox cassette[31] downstream of the GreenLantern, but this feature was not used in this study. This vector was then used by Monash Genome Modification Platform for Flp-mediated cassette exchange (Suppl. Fig. 3a) into clones #56, 62 and 32 of *Igs7*-targeted G4 ES cells (MG36, see above). 30µg pCAG-FlpO-IRES-Puro + 10µg AR157 were mixed with 0.8ml of ESC suspension at ~1×10^7/ml and transferred to a 4mm cuvette. After incubation at RT for 5 min, they were electroporated by applying a single pulse (each clone was divided into two sets: one pulsed with an exponential-decay pulse at 250V, 500µF capacitance, another one pulsed with a square-wave pulse at 250V, 5ms duration) followed by 5min at RT, then added into a 10cm dish pre-coated with mouse embryonic fibroblasts (MEFs). 1 day after transfection, transfection efficiency was checked under the fluorescent microscope, and drug selection was started (150µg/ml hygromycin). At 4 days after transfection, selection was changed to 100µg/ml hygromycin. At 6 days after transfection, we picked up 4 clones from each parental clone (#56-1 to 4, #62-1 to 4, #32-1 to 4) to MEF-coated 24-well plates. These clones were genotyped by 5'-GT PCR, 3'-GT PCR and TRE-GL specific PCR (see below). All clones were correctly targeted (Suppl. Fig. 3b).

465

ES1 5'-GT PCR (245bp) 64ºC	
MG36 5'-GT step2 up	CGACCTCTAGAAGTAAGCTTTGAGC
MG36 5'-GT step2 down	CCTCCCCTGGCACAACGTAA
ES1 3'-GT PCR (449 bp) 64ºC	
MG36 3'-GT step2 up	ATCTTAGCCAGACGAGCGGG
MG36 3'-GT step2 down	AATGACCGCTGTTATGCGGC
TRE-GL GT PCR (448 bp) 62ºC	
TRE-GL GT up	GTGAACCGTCAGATCGCCTG
TRE-GL GT down	TGGATCCTTAGCGCTGGTGT

466

467 Clones #62-1, 62-2, 56-1 and 56-2 were used for two sessions each of blastocyst microinjection. Males ET6
468 (clone 62-1, 85% chimera), ET28 (clone 62-2, 85% chimera), ET51 (clone #56-1, 80% chimera), ET59 (clone
469 #56-2, 80% chimera) were selected for breeding to next generation. Line #56-2 was crossed with *Gli1*^{CreER}
470 animals to establish the *Gli1*^{CreER}*; Tigre*$^{TRE\text{-}nGL}$ lines. 6 more highly chimeric males were kept as back-up
471 breeders.

472 Pulse of nuclear GFP expression in cartilage: *Gli1*$^{CreER/CreER}$*; Tigre*$^{TRE\text{-}nGL/TRE\text{-}nGL}$ female mice were time-mated
473 with *Col2a1-rtTA/+*; *R26*$^{LSL\text{-}tdTom/LSL\text{-}tdTom}$ male mice. The day of vaginal plug detection was deemed as
474 E0.5, and E19.5 was referred to as P0. Experimental set 1: Pregnant females were administered
475 doxycycline hyclate (Sigma) in drinking water (1mg/ml, with 0.5% sucrose for palatability) and
476 doxycycline hyclate food (Specialty feeds SF08-026, 600mg/Kg) from E12.5 to E13.5. Tamoxifen
477 (Sigma, 20 mg/ml in corn oil) was administered by oral gavage (180µg/g) at E13.5. Mouse embryos
478 were collected at E14.5, E17.5, P0, P14, P21. Experimental set 2: idem, except that Dox was given
479 from E17.5 to E18.5, and offspring was collected at P0, P14, P21 and P30. Limbs are dissected
480 carefully from the body, then fixed in 4% paraformaldehyde (PFA) for 2 days at 4ºC. Decalcification
481 was performed for P14, P21 and P30 samples by immersing them in 0.45M ethylenediaminetetraacetic
482 acid (EDTA) in PBS from 10-14 days at 4ºC.

483 RGBow experiments: *Gli1*$^{CreER/CreER}$ females were time-mated with *R26*$^{RGBow/RGBow}$ males. Experimental set 1:
484 Pregnant females were administered Tamoxifen by oral gavage at E12.5 (180 µg/g). Mouse embryos
485 were collected at E14.5, E16.5, P0, P1, P14, P30. Experiments 2: Pregnant females were administered
486 Tamoxifen (Sigma, 180ug/g in corn oil) by oral gavage at E13.5. Mouse embryos were collected at
487 E14.5, E15.5, E17.5, P0, P1, P14, P30. Limbs are dissected carefully from body, then fix limbs into
488 4% paraformaldehyde (PFA) for 2 days at 4ºC. Decalcification was performed on P14, P21, and P30
489 sample by immersing the specimens in 0.45M ethylenediaminetetraacetic acid (EDTA) in PBS from
490 10-14 days at 4ºC. An identical approach was used when using *Pdgfra*$^{CreER/+}$ females.

491 *X-gal staining*

492 For enzymatic detection of b-galactosidase activity, the frozen sections were postfixed 5 min with 4%
493 paraformaldehyde (PFA, Electron Microscopy Sciences) in PBS at RT. After PBS washes, the sections were
494 incubated 2 x 5 min with X-gal buffer (2 mM $MgCl_2$, 0.02% NP40 and 0.05% deoxycholate in PBS 0.1 M pH
495 7.4) and then overnight at 37ºC in X-gal reaction buffer (20 mg/ml X-gal, 5 mM $K_4Fe(CN)_6$ and 5 mM
496 $K_3Fe(CN)_6$ in X-gal wash buffer). After PBS rinses, the sections were postfixed 10 min in 4% PFA and PBS-
497 rinsed again. The sections were then counterstained with Nuclear Fast Red 0.005% for 15 min, serially
498 dehydrated, incubated 3 x 1 min with xylene, and cover-slipped using DPX mountant (Fisher).

499

500 *Single-nuclei RNA sequencing of Left-Cart-p21 model*

501 Sample preparation: *Pitx2-Cre/Cre; Col2a1-rtTA/+; Col2a1-eCFP/+* females were crossed with *Tigre*$^{Dragon\text{-}p21/Dragon\text{-}p21}$
502 males and given Dox (1mg/ml in drinking water with 0.5% sucrose) at E12.5. The knee region
503 (obtained via orthogonal cuts from the hypertrophic region of the distal femur to the hypertrophic region of the

504 proximal tibia in skinned hindlimbs) of E16.5 Left and Right limbs from uCtl and *Left-Cart-p21* samples (2
505 embryos of each genotype) were collected in DMEM with 10% DMSO and 5% calf serum, stored in a MrFrosty
506 (ThermoFisher) at 4ºC for 10 min and then transferred to -80ºC overnight. Tissue lysis and nuclei isolation were
507 done as described by L.G.M. in https://www.protocols.io/view/frankenstein-protocol-for-nuclei-isolation-from-
508 f-5jyl8nx98l2w/v2, in two batches of four samples each (left and right knees from one control and one
509 experimental embryo). Once ~5,000 nuclei per sample were collected, we proceeded with the 10x protocol
510 described in https://www.10xgenomics.com/support/single-cell-gene-expression/documentation/steps/library-
511 prep/chromium-single-cell-3-reagent-kits-user-guide-v-3-1-chemistry, minimizing the time between nuclei
512 preparation/sorting and chip loading. One chip per batch was used (4 channels in each case, to load left and right
513 samples from one control and one experimental embryo).

514 Sequencing and post-processing: The libraries were sequenced twice on Novaseq (800 million clusters/read
515 pairs each time, which when combined amounted to ~40,000 reads per nuclei across the 8 samples). Following
516 sequencing, fastq reads were mapped against a custom reference that combined Mus musculus (GRCm38) with
517 transgenic genes (tdTomato, ECFP, and WPRE) using CellRanger (v7.1.0). The resulting aligned reads were
518 analysed via R (4.0.2). Seurat (v.4.2.1) and R/Bioconductor SingleCellExperiment packages were used to
519 generate count matrices. For each sample, the mean of unique molecular identifiers (UMIs) (nCounts) was
520 calculated and used as a threshold to exclude empty droplets. Filtering was manually done according to the
521 nCount and number of genes. DoubletFinder (v2.0.3) was used to remove the expected doublets in each sample.
522 Harmony R package (v0.1.0) was also used to mitigate remove batch effects, and subsequently the data were
523 consolidated into a single Seurat object.

524 Seurat analyses: To identify the appropriate resolution, Clustree v 0.5.0 and Cluster Correlation analysis were
525 used. Visual representation of cluster assignments for individual cells was achieved within a reduced-
526 dimensional space using UMAP. To pinpoint the differentiation marker genes in the specific cluster as compared
527 to the remaining clusters, Wilcoxon Rank-Sum Test was used. This analysis was conducted using the
528 "FindAllMarkers" function within Seurat (v.4.2.1), P-value of less than 0.05 and only.pos = T, and a log-fold
529 change threshold of 0.1. To identify the cell type annotation, the clusters were mapped with mouse single cell
530 hindlimb data provided by https://doi.org/10.1038/s41586-023-06806-x. In addition, previously reported
531 cellular biomarkers and Gene Ontology (GO) annotations were utilized to annotate the cell clusters. The top 100
532 marker genes were utilized to enrich Gene Ontology (GO) terms through the ClusterProfiler package (version
533 3.14.3). To identify and confirm the cell type, GSEA comparison was also performed using SCP package (V.
534 0.5.1).

535 *Single-cell RNA-sequencing of Cart-p21 model*

536 Sample preparation, collection, and sequencing: Female *Gli1*$^{CreER/CreER}$ mouse was crossed with *Col2a1-rtTA/+;*
537 *Tigre*$^{TRE\text{-}p21/TRE\text{-}p21}$; *R26*$^{LSL\text{-}tdT/LSL\text{-}tdT}$ males. At E12.5, the pregnant mouse was given doxycycline in water (1 mg/ml
538 with 0.5% sucrose) and food (600 mg/kg), and Tamoxifen was orally gavaged (120 µg/g) at E13.5. At E14.5, the
539 embryos were collected and a tail sample used for genotyping. Sex and rtTA genotyping were performed using a
540 quick PCR protocol while the hindlimbs were carefully dissected. The dissected limbs then underwent treatment
541 with Accumax (ThermoFisher) in a rocker at 31ºC for 25 minutes and every 10 min, the samples were gently
542 shaken. The supernatant, containing homogenised soft tissues, was transferred into an 1.5-ml DNA LoBind®
543 Eppendorf tube and placed on ice for preservation, while the cartilaginous portions were exposed to Collagenase
544 B (5 mg/ml; Sigma) for ~90 min at 37ºC in a water bath (pipetted up and down every 20 min using Rainin wide
545 bore pipette tips). To stop collagenase activity, we then added 700 µl of cold DMEM+20% FBS for each tube.
546 We then combined soft- and cartilage-tissue homogenates, and the samples were diluted in 20 volumes of RBC
547 lysis buffer and rocked for 10 min at RT. The cells were then centrifuged at 500 g for 5 min at 4ºC and the cell
548 pellet was suspended in 900 µl of PBS + 0.05% BSA. After re-washing, the cells were resuspended in 400 µl of
549 PBS + 0.05% BSA. At the end, the cell suspension was filtered through 40-µm Flowmi® Cell Strainers and cells
550 were stained with DAPI (0.05 µg/ml) and transferred into Falcon™ Round-Bottom Polypropylene (Fisher
551 Scientific). The DAPI-negative, tdT^+ and tdT^- cells were sorted using flow cytometry (nozzle size of 100 µm,
552 operating at a PSI of 20 and a BOP of 223).

553 In total, two experimental males, two control males, two control females, and one experimental female were
554 utilized. The cells were counted by an automated cell counter (ThermoFisher) using trypan blue staining and all
555 passed at least 90% cell viability. Then, the cell suspensions were centrifuged at 500 g for 5 min at 4ºC and
556 resuspended in a smaller volume. The samples were then multiplexed based on sex. Specifically, for S1, tdT^+ EM
557 (Experimental Male) and tdT^+ CF (Control Female) cells were combined, totalling 7,500 cells. For S2, tdT^- EM
558 and tdT^- CF cells were combined, amounting to 25,000 cells (1000 cells/µl in a volume of 25 µl). In S3, tdT^+ EF
559 (Experimental Female) and tdT^+ CM (Control Male) cells were combined, totalling 5,700 cells. Finally, in S4,
560 tdT^- EF and CM cells were combined, comprising 24,000 cells. The libraries were prepared using Chromium
561 Next GEM Single Cell 3' Reagent Kits v3.1 (10X Genomics) according to manufacturer's directions and then
562 sequenced on Illumina (~833 million clusters/read pairs each time) with a length of 100 bp. All cDNA samples
563 passed the quality control.
564
565 scRNA-seq preprocessing: The fastq files were aligned against a custom reference comprising *Mus musculus*
566 (GRCm38; obtained from 10X Genomics Ref.) along with transgenic genes (tdTom, CreERT2, and WPRE) using
567 CellRanger (v7.2.0). In total, more than 98.2% of Reads Mapped to Genome and 25,190 genes were detected as
568 well as transgenes. To eliminate contaminated cells with ambient RNA, CellBender V 0.3.0 was used. The
569 expected number of genuine cells and total droplets were estimated based on the CellRanger output, using the
570 Raw_feature_bc_matrix.h5 file as input. Identified unique molecular identifiers (UMIs) were then mapped and
571 subset from the Seurat object generated by the filtered feature barcode matrix file. DoubletFinder (v2.0.3)[32] was
572 then used to remove expected doublets in each sample, with pK calculated separately for each sample. Then the
573 cells with low nCount_RNA and nFeature_RNA were filtered out.

574 *Testing for differences in cell type proportions*: To analyse the distinct cellular compositions among conditions,
575 the propeller test available in the speckle R (v.0.0.1, accessible at https://github.com/Oshlack/speckle) was
576 employed. The groups were classified with a false discovery rate (FDR) of ≤ 0.1 as indicative of notable variations
577 in cell types.

578 *Pseudo-time trajectory analysis*:

579 - RNA Velocity: The output files from CellBender (scRNA-seq) and CellRnager(snRNA-seq) were used as an
580 input for velocyto to generate a loom file including both spliced and unsliced sequence reads. Reads that passed
581 quality control after clustering were used as input for the velocyto command line implementation. The mouse
582 repeat annotation file (repeat_msk_srt.gtf) was obtained from the UCSC Genome Browser. Downstream
583 analysis was done using scVelo (Version 0.2.5) according to pertinent tutorials (https://scvelo.readthedocs.io/).
584 To visualize, velocity embedding was estimated using dynamical modeling embedded on UMAP.

585 - Monocle3.0: Cells from all condition sets were separately subjected to analyze using Monocle3.0 (version
586 1.2.9, https://github.com/cole-trapnell-lab/monocle3). The input data set was pre-processed by using
587 as.cell_data_set function and the object was converted to the monocle object. The cell trajectory was calculated
588 by using learn_graph function according to Monocle recommendation. The monocle resolution was determined
589 as 2 (k = 3) and then the cells ordered using learn_graph function. Using get_earliest_principal_node function,
590 the root was manually selected and then the pseudo-time trajectory graphs were visualized using plot_cells
591 function.

592 - Slingshot: We utilized the Slingshot[33] incorporated with SCP Package (0.5.6) for conducting pseudo-time–
593 based analysis of cell trajectories. The slingshot wrapper function incorporated UMAP dimensionality reduction
594 and cluster labels from Seurat objects to pinpoint the trajectory.

595 *EdU incorporation and detection*

596 A solution of 5-Ethynyl-2'-deoxyuridine (EdU) was prepared at 6.1 mg/ml in phosphate-buffered saline (PBS).
597 This solution was administered at a dose of 61 µg/g, subcutaneously (s.c) for pups and 30.5 µg/g
598 intraperitoneally (i.p.) for pregnant females, 1.5 hours before euthanizing the mice (or 2 days before, for pulse-
599 chase experiments). To detect EdU, a click chemistry reaction with fluorescein-conjugated azide (Lumiprobe

600 #A4130) was performed once the immunohistochemistry and/or TUNEL staining were completed on the same
601 slides. Briefly, the working solution was prepared in PBS, adding $CuSO_4$ (Sigma # C1297) to 4 mM, the azide
602 to 0.4 µM and freshly-dissolved ascorbic acid (Sigma #A0278) to 20 mg/ml, and incubating the sections for 15
603 min at room temperature in the dark, followed by PBS washes.

604 *Sample collection and processing*

605 Mouse embryos were euthanised using hypothermia in cold PBS, while mouse pups were euthanized by
606 decapitation. Upon collection of the embryos or pups, the limbs (including full tibiae and/or femora) were
607 carefully dissected out in cold PBS, skinned, and fixed in 4% paraformaldehyde (PFA) for 2 days at 4ºC.
608 Samples of P1 or younger were not subjected to decalcification. For P3, P5, and P7 samples, decalcification was
609 performed by immersing the specimens in 0.45M ethylenediaminetetraacetic acid (EDTA) in PBS for 3, 5, and
610 7 days, respectively, at 4ºC. Following several washes with PBS, the limb tissues were cryoprotected in PBS
611 containing 15% sucrose and then equilibrated in 30% sucrose at 4ºC until they sank. The hindlimbs were then
612 oriented sagittally, facing each other, with the tibiae positioned at the bottom of the block (closest to the blade
613 during sectioning) and embedded in Optimal Cutting Temperature (OCT) compound using cryomolds (Tissue-
614 Tek). The specimens were frozen by immersing them in dry-ice-cold iso-pentane (Sigma). Serial sections with
615 a thickness of 7 µm were collected with a Leica CM3050S Cryostat on Superfrost slides. The sections were
616 allowed to dry for at least 30 minutes and stored at -80ºC until further use. Prior to conducting histological
617 techniques, the frozen slides were brought to room temperature in PBS, and the OCT compound was washed
618 away with additional rounds of PBS rinses.

619 *Micro-CT and bone length analysis*

620 The micro-CT and bone length analysis was as previously described[34]. Briefly, samples were retained and fixed
621 in 4% PFA as residual tissues from other experiments in the Rosello-Diez lab. Whole femora and humeri were
622 scanned using a Siemens Inveon PET-SPECT-CT small animal scanner in CT modality (Monash Biomedical
623 Imaging). The scanning parameters included a resolution of 20 and 40 µm, 360 projections at 80 kV, 500 µA,
624 600-ms exposure with a 500-ms settling time between projections. Binning was applied to adjust the resolution
625 with 2×2 for 20-µm scans and 4×4 for 40-µm scans. The acquired data were reconstructed using a Feldkamp
626 algorithm and converted to DICOM files using Siemens software. For the analysis and bone length
627 measurements, Mimics Research software (v21.0; Materialize, Leuven, Belgium) equipped with the scripting
628 module was utilized to develop the analysis pipeline[34].

629 *Immunohistochemistry and TUNEL staining*

630 For antigen retrieval, the sections were subjected to citrate buffer (10 mM citric acid, 0.05% Tween 20 [pH 6.0])
631 at 90ºC for 15 minutes. Afterward, the sections were cooled down in an ice water bath, washed with PBSTx
632 (PBS containing 0.1% Triton X-100). To perform TUNEL staining, the endogenous biotin was blocked using
633 the Avidin/Biotin blocking kit (Vector #SP-2001) after antigen retrieval. Subsequently, TdT enzyme and Biotin-
634 16-dUTP (Sigma #3333566001 and #11093070910) were used according to the manufacturer's instructions.
635 Biotin-tagged DNA nicks were visualized using Alexa488- or Alexa647-conjugated streptavidin (Molecular
636 Probes, diluted 1/1000) during the incubation with the secondary antibody.

637 For immunohistochemistry staining, sections were incubated with the primary antibodies prepared in PBS for
638 either 1.5 hours at room temperature or overnight at 4ºC (see list of antibodies below). Following PBSTx washes,
639 the sections were incubated with Alexa488-, Alexa555-, and/or Alexa647-conjugated secondary antibodies
640 (Molecular Probes; diluted 1/500 in PBSTx with DAPI) for 1 hour at room temperature. After additional PBSTx
641 washes, the slides were mounted using Fluoromount™ Aqueous Mounting Medium (Sigma). The antibodies
642 used, along with their host species, vendors, catalogue numbers, and dilutions, were as follows: GFP (alpaca
643 nanobody, Chromotek #gba488, Alexa 488-conjugated), mKate2/TagRFP (rabbit polyclonal, Invitrogen
644 R10367, diluted 1/500), mCherry (goat polyclonal, Origene Technologies #AB0040-200, diluted 1/500, or rat
645 monoclonal, Thermofisher #M11217, diluted 1/500), p21 (rabbit polyclonal, SantaCruz biotechnologies sc-471,
646 diluted 1/300).

647 *In situ hybridisation*

648 To perform *in situ* hybridisation, sections were fixed in 4% PFA for 20 minutes at room temperature, washed in
649 PBS, and treated with 4µg/ml Proteinase K for 15 minutes at 37ºC. After washing in PBS, the sections were

650 refixed with 4% PFA, followed by treatment with 0.1N pH8 triethanolamine (Sigma #90279), 0.25% acetic
651 anhydride (Sigma #320102) for 10 minutes at room temperature. Subsequently, the sections were washed in
652 PBS and water and incubated with prehybridization buffer (50% formamide, 5x SSC pH 5.5, 0.1% 3-[(3-
653 Cholamidopropyl)dimethylammonio]-1-propanesulfonate (CHAPS), 0.05 mg/ml yeast tRNA, 0.1% Tween 20,
654 1x Denhardt's) at 60ºC for 30 minutes. The sections were then incubated with 1µg/ml preheated riboprobes and
655 subjected to hybridization at 60ºC for 2 hours. Post-hybridization washes were performed using post-
656 hybridisation buffer I (50% formamide, 5× SSC pH 5.5, 1% SDS) and II (50% formamide, 2× SSC pH 5.5, 0.2%
657 SDS) preheated at 60ºC for 30 minutes, respectively. The sections were then washed with maleic acid buffer
658 (MABT: 100mM maleic acid, 150mM NaCl, 70mM NaOH, 0.1% Tween 20) and blocked with 10% goat serum,
659 1% blocking reagent (Roche #11096176001) in MABT at room temperature for 30 minutes. Next, the sections
660 were incubated overnight at 4ºC with anti-digoxigenin-AP (Sigma #11093274910) diluted 1/4000 in MABT
661 with 2% goat serum and 1% blocking reagent. After several MABT washes, the sections underwent incubation
662 with Alkaline Phosphatase (AP) buffer (0.1M Tris-HCL pH 9.5, 0.1M NaCl, 0.05M $MgCl_2$, 0.1% Tween 20),
663 with the second one containing 1mM levamisole and then developed colour using BM purple (Roche
664 #11442074001) at 37ºC. Following one wash in PBS, the sections were fixed for 10 minutes in 4% PFA,
665 counterstained with Nuclear Fast Red (Sigma #N3020) at room temperature for 10 minutes, and rinsed in water.
666 Dehydration was performed by passing the sections through 70% ethanol, 90% ethanol, absolute ethanol (thrice),
667 and xylene (twice). Finally, the sections were mounted with DPX (Sigma #100579).

668 *Hybridization chain reaction (HCR)*

669 The slides were thawed for 20 min in RNAse-free PBS (DPBS; GIBCO, Invitrogen, LOT: 866200), then were
670 rinsed twice with DPBS (devoid of Ca^{2+}/Mg^{2+}) and fixed in ice-cold 4% PFA for 15 min at 4ºC. The samples
671 were then dehydrated by being immersed in 50% ethanol, 75% ethanol, and 100% ethanol for 5 min at RT. The
672 slides were washed with DPBS. A total of 200 µL of probe hybridization buffer was added on the sample and
673 incubated for a minimum of 10 min at 37ºC. After draining the excess buffer, 100 µL of hybridization buffer
674 with 16 nM of each probe were added to the slide and the incubation was carried out for at least 12 hours.

675 To eliminate any excess probes bound to the sample, the slides underwent a series of washes as follows: i) 75%
676 wash buffer:25% 5× SSCT for 15 minutes; ii) 50% wash buffer:50% 5× SSCT for 15 minutes; iii) 25% wash
677 buffer:75% 5× SSCT for 15 minutes; iv) 100% 5× SSCT for 15 minutes. Following the previous wash steps, the
678 slides were immersed in 100% 5× SSCT for 5 minutes at room temperature. Pre-amplification was performed
679 by adding 200 µL of amplification buffer on top of the sample, and incunbating in a humidified chamber for 30
680 minutes at room temperature. Meanwhile, 6 pmol of hairpin h1 and 6 pmol of hairpin h2 (2 µL of a 3 µM stock
681 per slide) were separately prepared by heating them at 95ºC for 90 seconds and cooled to room temperature in
682 a dark drawer for 30 minutes. Each hairpin was added to 100 µL of amplification buffer at room temperature.
683 After removing the pre-amplification solution from the slides, 100 µL of the hairpin solution was added on top
684 of the samples, and incubation was carried out for a minimum of 12 hours in a dark, humidified chamber at room
685 temperature. Subsequently, the slides were washed twice with 5× SSCT at room temperature for 30 minutes.
686 Finally, the samples were washed for 5 minutes with 5× SSCT at room temperature. Following these, the slides
687 were allowed to dry and then mounted using antifade mounting reagent (Fluoromount-G™ Mounting Medium,
688 Cat: 00495802, Thermosfisher).

689 *Imaging*

690 Sagittal sections of the limbs were captured, with a focus on the area between the distal femora and proximal
691 tibiae. Typically, at least 2 sections per limb were analysed, although in most cases 4 sections were examined.
692 In the case of cultured distal femora, frontal sections were used as they provided better identification of the
693 different epiphyseal regions. To determine the boundaries of the resting zone (RZ), proliferative zone (PZ) and
694 hypertrophic zone (HZ), morphological criteria were applied. The transition between round (resting) and flat
695 (columnar) nuclei, forming an arch along the upper point of the grooves of Ranvier, was considered as the start
696 of the PZ. On the other hand, the transition towards larger, more spaced nuclei (pre-hypertrophic) marked the
697 end of the PZ. The point where the pericellular matrix exhibited a sharp reduction around enlarging chondrocytes
698 was designated as the beginning of the HZ. The distal end of the last intact chondrocyte served as the endpoint

of the HZ. For imaging, bright-field and fluorescence images were acquired using a Zeiss inverted microscope (Imager.Z1 or Z2) equipped with ZenBlue software. Mosaic pictures were automatically generated by assembling individual tiles captured at 10× magnification for bright-field images and 20× magnification for fluorescence images.

Image analysis and quantification

The regions of interest such as resting, proliferative and hypertrophic zones (RZ, PZ, HZ) and the secondary ossification centre (SOC) were identified from imaged sections of the multiple models (left and right; experimental and control proximal tibial cartilage). Consistent parameters such as brightness, contrast, filters and layers were kept the same for all the images in the same study.

Cell count analysis

The RZ and PZ were identified and segmented from sections stained for DAPI, tdTomato, and TUNEL or EdU using FIJI software. The number of cells in the region of interest (RZ & PZ) was measured using CellProfiler. The exact pipelines are available upon request.

Statistical analysis

Statistical comparisons were performed using appropriate tests based on the experimental design. An unpaired t test was used for comparisons involving one variable and two conditions. Two-way ANOVA was utilized for comparisons involving two variables and two or more conditions. Non-parametric tests were selected when the assumption of normality could not be met. All statistical analyses were conducted using Prism10 software (GraphPad).

Conflict of Interest

F.J.R. receives institutional support as a coinvestigator and subcontracted by the Peter MacCallum Cancer Centre for an investigator-initiated trial which receives funding support from Sanofi/Regeneron Pharmaceuticals. R.W.J. reports grants and personal fees from MycRx outside the submitted work. The rest of the authors declare that the research was conducted in the absence of any commercial or financial relationships that could be construed as a potential conflict of interest.

Author Contributions

X.Q.: data acquisition and analysis, supervision; E.R.: data acquisition, analysis, figure preparation, manuscript drafting; C.H.H: data acquisition and analysis, figure preparation; K.K.V.: data acquisition, analysis, figure preparation; L.G.M.: experimental design, data acquisition; F.J.R.: experimental design, data analysis; M.Z: data analysis; R.W.J: funding acquisition, supervision; S.L.A.: data analysis, manuscript editing, supervision; D.R.P.: data analysis, supervision; A.R-D.: conceptualization, experimental design, data analysis, funding acquisition, supervision, figure preparation, manuscript drafting and editing.

Funding

HFSP CDA00021/2019-C (to A.R-D.) and NHMRC Ideas grant 2002084 (to A.R-D. and C.H.H.). The Australian Regenerative Medicine Institute is supported by grants from the State Government of Victoria and the Australian Government. The Novo Nordisk Foundation Center for Stem Cell Medicine, reNEW, is supported by a Novo Nordisk Foundation grant number NNF21CC0073729.

Acknowledgments

We acknowledge the Monash Genomics and Bioinformatics Platform for their excellent technical help, as well as the Monash Genome Modification Platform, for their help with gene targeting and genotyping strategy (design and execution). We thank Timothy Semple for his help with library preparation for the snRNA-seq dataset.

Data Availability Statement

The single-nuclei and single-cell RNA-seq datasets have been deposited at the NCBI Sequence Read Archive (SRA) with accession numbers PRJNA1136579 and PRJNA1138445, respectively.

References

744 1 Lander, A. D., Gokoffski, K. K., Wan, F. Y., Nie, Q. & Calof, A. L. Cell lineages and the logic
745 of proliferative control. *PLoS Biol* **7**, e15 (2009). https://doi.org:10.1371/journal.pbio.1000015

746 2 Newton, P. T. *et al.* A radical switch in clonality reveals a stem cell niche in the epiphyseal
747 growth plate. *Nature* **567**, 234-238 (2019). https://doi.org:10.1038/s41586-019-0989-6

748 3 Rolian, C. Endochondral ossification and the evolution of limb proportions. *Wiley*
749 *interdisciplinary reviews. Developmental biology*, e373 (2020).
750 https://doi.org:10.1002/wdev.373

751 4 Kronenberg, H. M. Developmental regulation of the growth plate. *Nature* **423**, 332-336 (2003).
752 https://doi.org:10.1038/nature01657

753 5 Zhou, X. *et al.* Chondrocytes transdifferentiate into osteoblasts in endochondral bone during
754 development, postnatal growth and fracture healing in mice. *PLoS Genet* **10**, e1004820 (2014).
755 https://doi.org:10.1371/journal.pgen.1004820

756 6 Maes, C. *et al.* Osteoblast precursors, but not mature osteoblasts, move into developing and
757 fractured bones along with invading blood vessels. *Dev Cell* **19**, 329-344 (2010).
758 https://doi.org:10.1016/j.devcel.2010.07.010

759 7 Karlsson, C., Thornemo, M., Henriksson, H. B. & Lindahl, A. Identification of a stem cell
760 niche in the zone of Ranvier within the knee joint. *J Anat* **215**, 355-363 (2009).
761 https://doi.org:10.1111/j.1469-7580.2009.01115.x

762 8 Mizuhashi, K. *et al.* Resting zone of the growth plate houses a unique class of skeletal stem
763 cells. *Nature* **563**, 254-258 (2018). https://doi.org:10.1038/s41586-018-0662-5

764 9 Muruganandan, S. *et al.* A FoxA2+ long-term stem cell population is necessary for growth
765 plate cartilage regeneration after injury. *Nature communications* **13**, 2515 (2022).
766 https://doi.org:10.1038/s41467-022-30247-1

767 10 Ono, N., Ono, W., Nagasawa, T. & Kronenberg, H. M. A subset of chondrogenic cells provides
768 early mesenchymal progenitors in growing bones. *Nature cell biology* **16**, 1157-1167 (2014).
769 https://doi.org:10.1038/ncb3067

770 11 Pineault, K. M., Song, J. Y., Kozloff, K. M., Lucas, D. & Wellik, D. M. Hox11 expressing
771 regional skeletal stem cells are progenitors for osteoblasts, chondrocytes and adipocytes
772 throughout life. *Nature communications* **10**, 3168 (2019). https://doi.org:10.1038/s41467-019-
773 11100-4

774 12 Matsushita, Y. *et al.* Hes1 marks peri-condensation mesenchymal cells that generate both
775 chondrocytes and perichondrial cells in early bone development. *J Biol Chem* **299**, 104805
776 (2023). https://doi.org:10.1016/j.jbc.2023.104805

777 13 Li, B. *et al.* Gli1 labels progenitors during chondrogenesis in postnatal mice. *EMBO reports*
778 (2024). https://doi.org:10.1038/s44319-024-00093-x

779 14 Ahn, S. & Joyner, A. L. Dynamic changes in the response of cells to positive hedgehog
780 signaling during mouse limb patterning. *Cell* **118**, 505-516 (2004).
781 https://doi.org:10.1016/j.cell.2004.07.023

782 15 Madisen, L. *et al.* A robust and high-throughput Cre reporting and characterization system for
783 the whole mouse brain. *Nat Neurosci* **13**, 133-140 (2010). https://doi.org:10.1038/nn.2467

784 16 He, M. *et al.* Strategies and Tools for Combinatorial Targeting of GABAergic Neurons in
785 Mouse Cerebral Cortex. *Neuron* **92**, 555 (2016). https://doi.org:10.1016/j.neuron.2016.10.009

17 Fenichel, I., Evron, Z. & Nevo, Z. The perichondrial ring as a reservoir for precartilaginous cells. In vivo model in young chicks' epiphysis. *Int Orthop* **30**, 353-356 (2006). https://doi.org:10.1007/s00264-006-0082-2

18 Posey, K. L. *et al.* An inducible cartilage oligomeric matrix protein mouse model recapitulates human pseudoachondroplasia phenotype. *Am J Pathol* **175**, 1555-1563 (2009). https://doi.org:10.2353/ajpath.2009.090184

19 Ahmadzadeh, E. *et al.* A collection of genetic mouse lines and related tools for inducible and reversible intersectional misexpression. *Development* **147** (2020). https://doi.org:10.1242/dev.186650

20 H'Ng, C. H. *et al.* Compensatory growth and recovery of cartilage cytoarchitecture after transient cell death in fetal mouse limbs. *Nature communications* **15**, 2940 (2024). https://doi.org:10.1038/s41467-024-47311-7

21 Shi, Y. *et al.* Gli1 identifies osteogenic progenitors for bone formation and fracture repair. *Nature communications* **8**, 2043 (2017). https://doi.org:10.1038/s41467-017-02171-2

22 Harper, J. W., Adami, G. R., Wei, N., Keyomarsi, K. & Elledge, S. J. The p21 Cdk-interacting protein Cip1 is a potent inhibitor of G1 cyclin-dependent kinases. *Cell* **75**, 805-816 (1993).

23 Rosello-Diez, A., Madisen, L., Bastide, S., Zeng, H. & Joyner, A. L. Cell-nonautonomous local and systemic responses to cell arrest enable long-bone catch-up growth in developing mice. *PLoS Biol* **16**, e2005086 (2018). https://doi.org:10.1371/journal.pbio.2005086

24 Phipson, B. *et al.* propeller: testing for differences in cell type proportions in single cell data. *Bioinformatics* **38**, 4720-4726 (2022). https://doi.org:10.1093/bioinformatics/btac582

25 Losner, J., Courtemanche, K. & Whited, J. L. A cross-species analysis of systemic mediators of repair and complex tissue regeneration. *NPJ Regen Med* **6**, 21 (2021). https://doi.org:10.1038/s41536-021-00130-6

26 Shiratori, H., Yashiro, K., Shen, M. M. & Hamada, H. Conserved regulation and role of Pitx2 in situs-specific morphogenesis of visceral organs. *Development* **133**, 3015-3025 (2006). https://doi.org:10.1242/dev.02470

27 Chan, L. L., Huang, J., Hagiwara, Y., Aguila, L. & Rowe, D. Discriminating multiplexed GFP reporters in primary articular chondrocyte cultures using image cytometry. *J Fluoresc* **24**, 1041-1053 (2014). https://doi.org:10.1007/s10895-014-1383-2

28 Ahn, S. & Joyner, A. L. In vivo analysis of quiescent adult neural stem cells responding to Sonic hedgehog. *Nature* **437**, 894-897 (2005). https://doi.org:10.1038/nature03994

29 Chung, M. I., Bujnis, M., Barkauskas, C. E., Kobayashi, Y. & Hogan, B. L. M. Niche-mediated BMP/SMAD signaling regulates lung alveolar stem cell proliferation and differentiation. *Development* **145** (2018). https://doi.org:10.1242/dev.163014

30 Hamilton, T. G., Klinghoffer, R. A., Corrin, P. D. & Soriano, P. Evolutionary divergence of platelet-derived growth factor alpha receptor signaling mechanisms. *Mol Cell Biol* **23**, 4013-4025 (2003). https://doi.org:10.1128/MCB.23.11.4013-4025.2003

31 Pei, W. *et al.* Polylox barcoding reveals haematopoietic stem cell fates realized in vivo. *Nature* **548**, 456-460 (2017). https://doi.org:10.1038/nature23653

826 32 McGinnis, C. S., Murrow, L. M. & Gartner, Z. J. DoubletFinder: doublet detection in single-
827 cell RNA sequencing data using artificial nearest neighbors. *Cell systems* **8**, 329-337. e324
828 (2019).

829 33 Street, K. *et al.* Slingshot: cell lineage and pseudotime inference for single-cell transcriptomics.
830 *BMC Genomics* **19**, 1-16 (2018).

831 34 Beltran Diaz, S. *et al.* A new pipeline to automatically segment and semi-automatically
832 measure bone length on 3D models obtained by Computed Tomography. *Frontiers in Cell and*
833 *Developmental Biology* (2021).

834